

# ***The Large Greenland Landslide of 2017: Was a Tsunami Warning Possible?***

**by Wei-An Chao, Tso-Ren Wu, Kuo-Fong Ma, Yu-Ting Kuo, Yih-Min Wu, Li Zhao, Meng-Ju Chung, Han Wu, and Yu-Lin Tsai**

## **ABSTRACT**

Tsunamis generated by mass movements such as landslides, underwater slumps, and rock avalanches can lead to serious inundation of nearby populated areas. The lack of timely estimations of the moving mass volume, however, makes providing operational early warnings for landslides particularly challenging. In June 2017, a large landslide in Greenland generated tsunami waves of about 1 m high that impacted the small town of Nuugaatsiaq. We show how the seismic analysis of real-time seismic records from the Greenland Ice Sheet Monitoring Network (GLISN) can provide estimates of essential physical properties of the landslide such as collapse mass and sliding velocity shortly after origin time. The estimation of the landslide source parameters can be utilized for tsunami-wave simulations. We demonstrate how the real-time integration of seismic waveform inversion with forward tsunami-wave simulation could have enabled a timely operational warning (about 10 min) before the arrival of the impending tsunami waves at the village of Nuugaatsiaq.

## **INTRODUCTION**

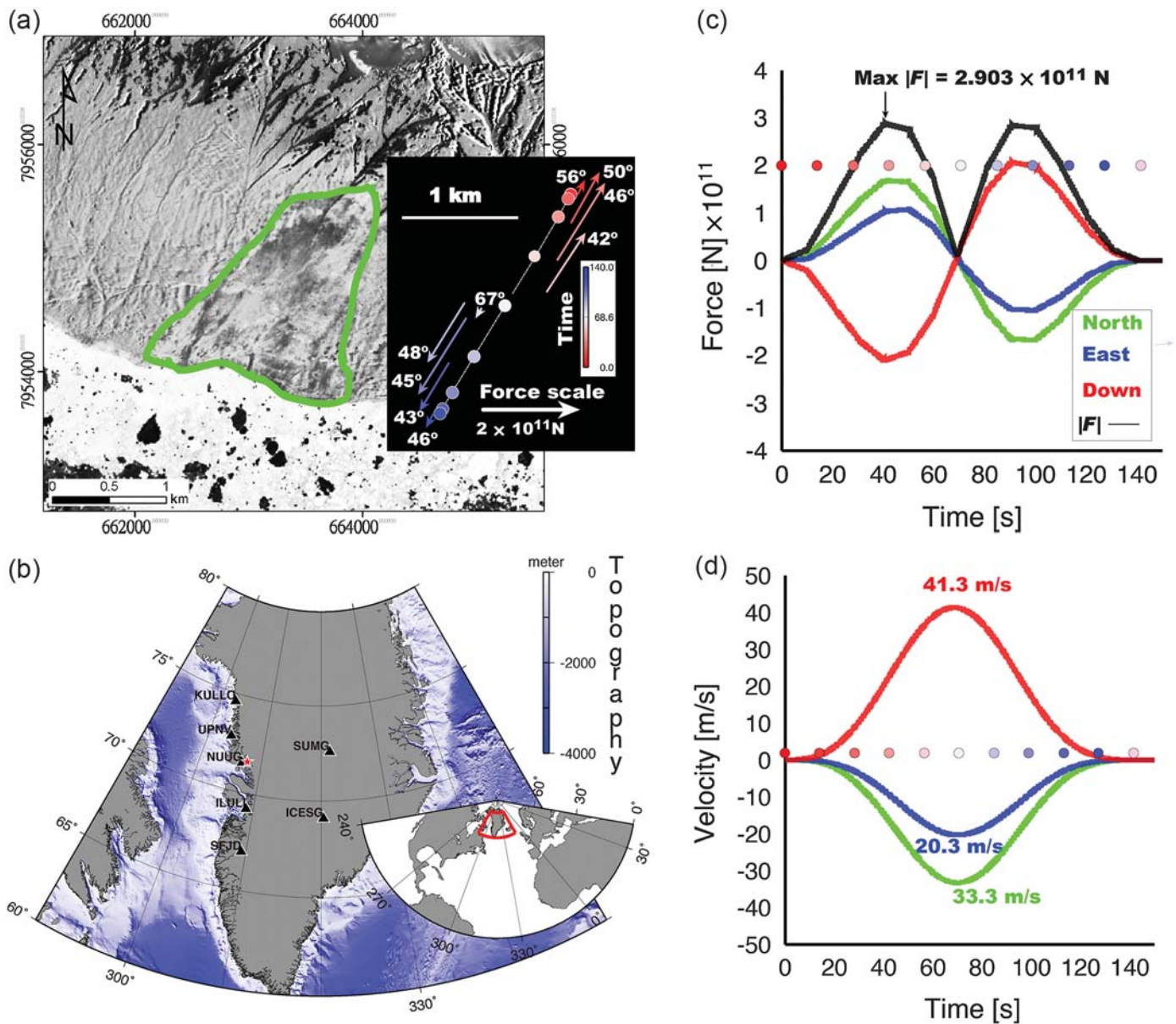
Gravity-induced mass movements such as landslides and rock avalanches pose a serious threat to human life. Rapidly moving landslide masses, for instance, can cause both human casualties and significant damage to infrastructure. Most landslide dams form when a mass of sediments and rock, eroded from mountain and hill slopes, blocks the river channels. A possible dam-breaking flood with high flow velocity also has the potential to destroy the downstream area (Costa and Schuster, 1988). Moreover, landslides occurring in coastal regions can generate potentially destructive tsunami waves when the sliding mass enters the water, which present serious hazards to coastal populations. On 17 June 2017, at 21:39 local time, a large landslide (2000 m long and 1100 m wide, Fig. 1a) occurred in Greenland when a landslide mass descended into the sea at Karrat Fjord. Differential digital elevation models (DEMs) estimate a landslide volume of 35–51 million cubic meters ( $3.5\text{--}5.1 \times 10^7 \text{ m}^3$ ). The landslide triggered a tsunami that washed up in a remote region near the village of Nuugaatsiaq, reportedly killing four people, injuring dozens, and washing away eleven homes (Bessette-Kirton *et al.*, 2017).

This tsunami-generating landslide in Greenland raised a pressing question: Can we detect in time the potential tsunami hazard of landslide events and issue warnings before the arrival of destructive tsunami waves? Early warning for landslide-generated tsunami is particularly challenging due to the lack of information on properties, such as collapsing mass, needed to run numerical simulations. Fortunately, seismic stations can detect long-period (LP, 20–150 s) seismic waves generated by landslide sources due to the unloading and reloading cycle of Earth mass, which can be detected by the seismic stations (Allstadt, 2013; Ekström and Stark, 2013; Chao *et al.*, 2016). We can then use real-time seismic signals generated by landslides to rapidly determine the occurrence time, collapse mass, source mechanisms, and runout path of the landslide events. In Taiwan, where massive landslides occur every year, these procedures have been implemented already (Chao *et al.*, 2017).

In the current study area, the Greenland Ice Sheet Monitoring Network (GLISN, see Data and Resources) has installed seismic sensors to monitor the dynamic behavior of the Greenland ice sheet as it relates to climate change. Despite the absence of direct observations of the Greenland landslide, this network provides valuable information about the event. Poli (2017) first reports the observation of seismic precursors to the Greenland landslide from a seismic station NUUG of the GLISN network. Here, we present the seismic data available within a few hundred kilometers from the source of the Greenland landslide and how we applied LP waveform inversion to derive information on the landslide dynamics and its collapse volume. Using the landslide volume and assuming that most of the material slides into the ocean in the tsunami simulation, we can simulate the tsunami waves potentially generated in the area. We propose the possibility of a new near-real-time system to rapidly warn of the tsunami hazard posed by occurrence of catastrophic coastal landslides in the world by integrating the analysis of seismic data from the Global Seismographic Network (GSN) with tsunami modeling techniques.

## **SENTINEL-2 IMAGES AND SEISMIC DATA**

The European Space Agency (ESA) developed Sentinel-2 as a wide-swath high-resolution multispectral optical Earth observation mission as part of the European Copernicus program.

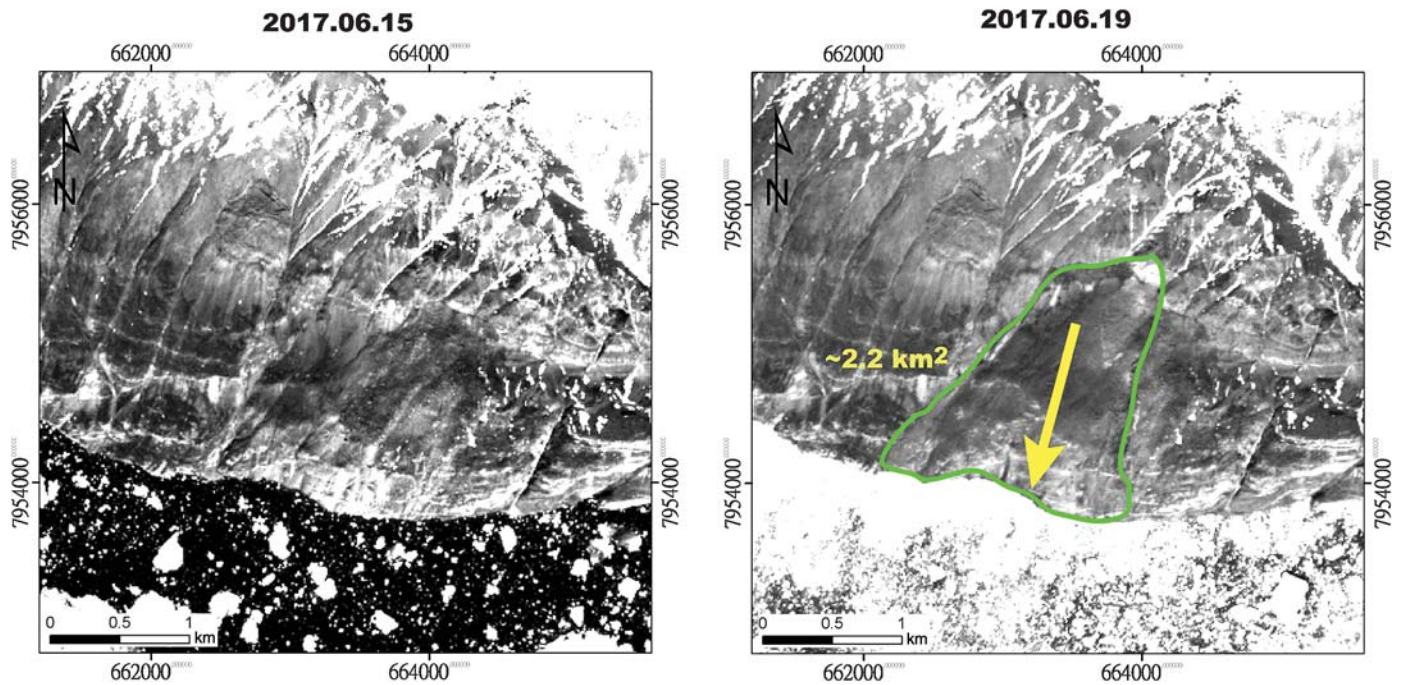


▲ **Figure 1.** (a) Gray-scale distribution map of pixel differences between the pre- and post-landslide Sentinel-2 images. The green line delimits the landslide collapse area. The inner panel shows the locations of the block mass along the seismically inferred trajectory. Arrows indicate the time-dependent horizontal force vectors acting on the Earth surface, with the same color scheme for the time progression shown by the dots. Degree values designate the dipping angles of the sliding forces. (b) Map showing the positions of seismic stations (triangles) and the landslide (red star). (c) Three-component long-period force–time history (LFH) of the Greenland landslide. Time progression from 0 to 140 s is shown by dots with different colors. (d) 3D velocity–time history computed directly from the LFH in (c) with an estimated collapse mass ( $m$ ) of  $1.9 \times 10^{11}$  kg.

The multispectral instrument constitutes 4, 6, and 3 spectral bands with a spatial resolution of 10, 20, and 60 m, respectively. Because this system provides images for the same location every five days (Drusch *et al.*, 2012), we obtained Sentinel-2 level-1c images (Fig. 2) before (15 June 2017) and after (19 June 2017) the Greenland landslide from the ESA website (see [Data and Resources](#)). The data processing of level-1c images includes both radiometric and geometric corrections with a resulting uncertainty of about 20 m (Drusch *et al.*, 2012). Based on

the Sentinel-2 images, we can directly map the collapsed landslide mass as having an area of 2.2 km<sup>2</sup>, as shown in Figures 1a and 2. The landslide areas mapped from these images serve to validate the seismically inferred parameters, including the run-out path and force vectors of the sliding mass (Fig. 1a).

The GLISN project deployed 19 seismic stations throughout the island to investigate the interactions between the Greenland ice sheet and climate dynamics. Most of the stations were equipped with Guralp CMG-3Ts and Streckeisen STS-2



▲ **Figure 2.** Analysis of Sentinel-2 satellite images with a spatial resolution of 10 m (left) before and (right) after the Greenland landslide. The arrow indicates the direction of the sliding force of the landslide event as determined in this study. The green line delimits the landslide collapse area. Images provided by the European Space Agency (Drusch *et al.*, 2012).

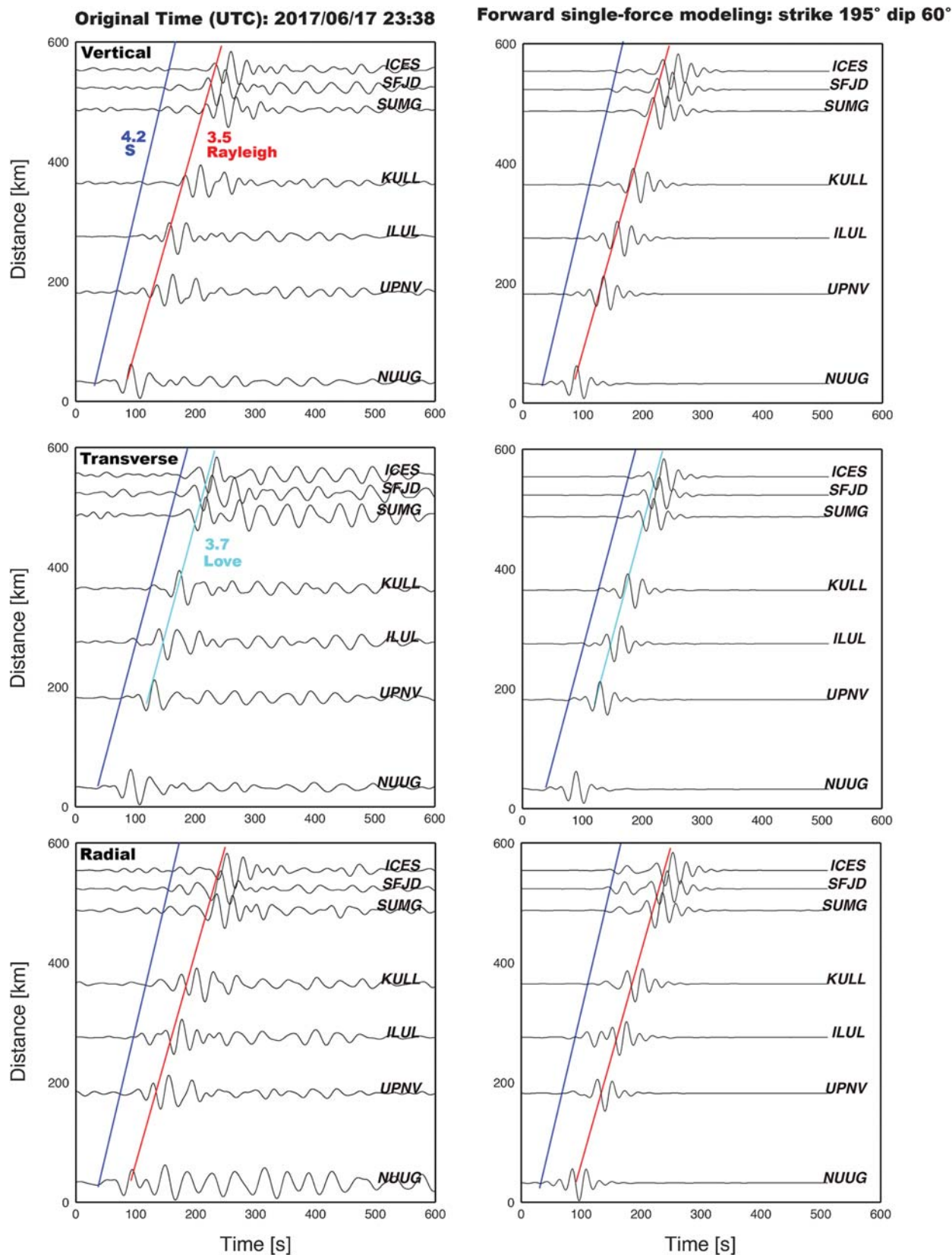
broadband seismometers. In our study, we used records from seven stations (Fig. 1b) retrieved from the Incorporated Research Institutions for Seismology Data Management Center (IRIS-DMC). Seismic data processing then involved removing the instrument responses, record means, and linear trends; integrating ground velocities to displacements; rotating the horizontal records to the radial and transverse directions at each station; and band-pass filtering to the LP (20–50 s) range. Visual inspection suggests that seismic ground motions are best observed in the LP range. Treating the arrival time as a unique function of the event-to-station distance confirms that the observed arrivals correspond to those generated by the Greenland landslide event (Fig. 3). The seismic station NUUG, located 32 km to the southwest, and closest to the landslide area, recorded the arrival of the surface wave generated by the landslide at 23:39:30 UTC.

## METHODS

To estimate landslide properties such as mass and propagation speed, we employ an inversion algorithm for the landquake's LP force–time history (LFH) that calculates the LFH using multiple 3D time-dependent forces (Chao *et al.*, 2016). Waveform modeling is conducted by convolving the LFH model (seismic source time function) with the Green's functions (wave propagation effect) calculated for the 1D global average velocity model ak135 (Kennett *et al.*, 1995) using the propagator matrix approach (Zhu and Rivera, 2002). Inversion of the LFH is conducted by first assigning each recorded seismogram to a given confidence level depending on their signal-to-noise ratio (SNR),

and then maximizing the fitness between recorded and synthetic waveforms. We measure the level of fitness via both the normalized cross-correlation coefficient (CC values in Fig. 4) and the reduction in the variance (Chao *et al.*, 2016). Here, SNR is calculated from the ratio between peak envelope amplitude and whole-term average. Because of uncertainty in event occurrence time and the used velocity model, we note that a time shift of up to  $\pm 10$  s is allowed independently for each component to achieve the maximum normalized CC.

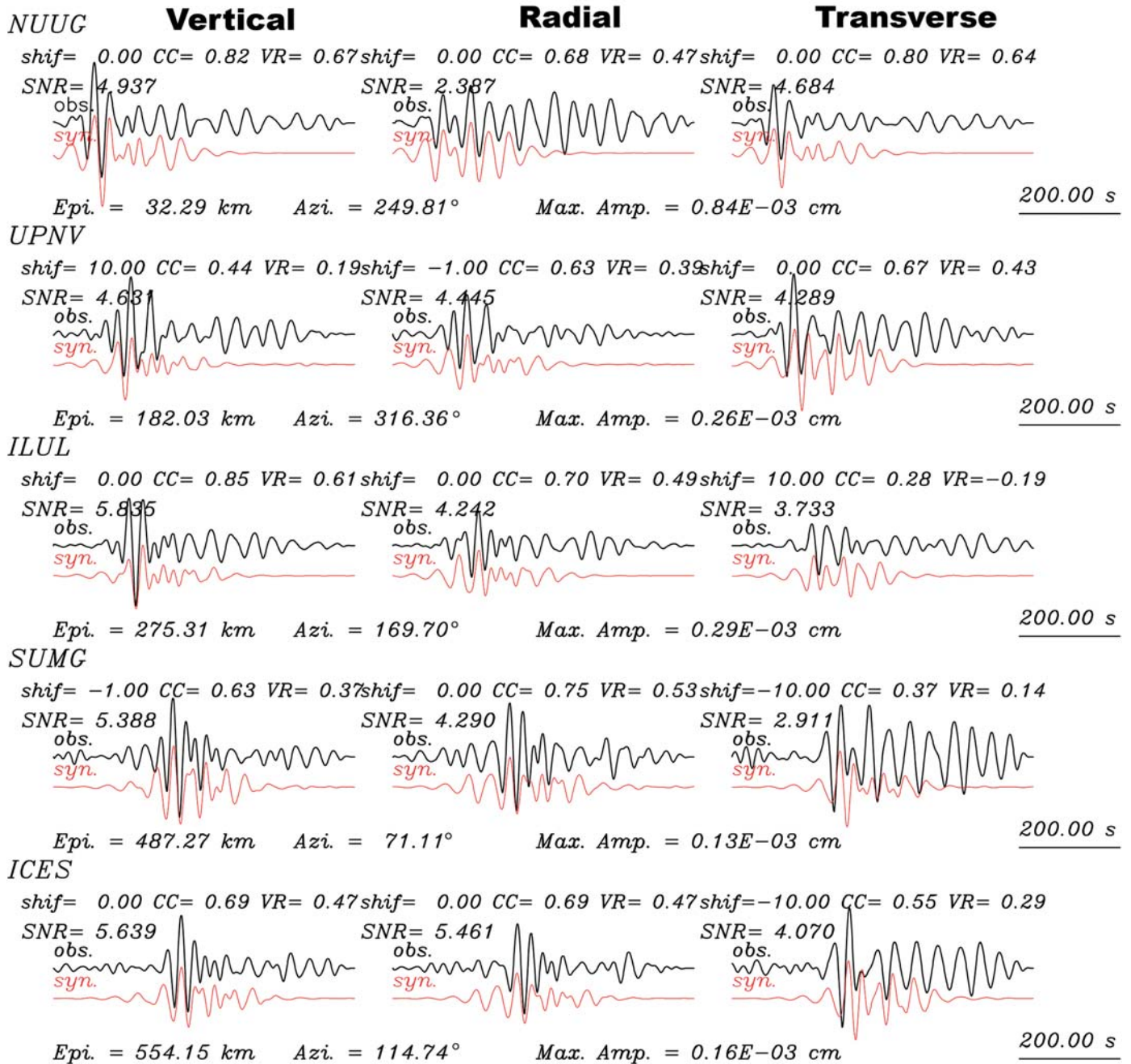
Near-real-time seismic analysis can provide a constraint on the volume of the mass materials involved in the slumping, thereby facilitating a timely simulation of the tsunami-wave generation and propagation. In this study, we simulate the tsunami generation and propagation by employing a well-validated tsunami modeling package, CORnell Multi-grid COupled Tsunami Model (COMCOT; Lin *et al.*, 2015). COMCOT solves the nonlinear shallow-water equation in a spherical coordinate system while accounting for Coriolis force. In this simulation, we used a resolution of 0.5 arcmin. We obtained the bathymetry data from GEneral Bathymetric Chart of the Oceans (GEBCO; see Data and Resources) database. Applying the scenario study method, we estimated the initial wave height of the landslide-generated tsunami by trial-and-error tests after constraining the wave height to 1 m, as observed in a video footage of the tsunami (see Data and Resources) taken by villagers. Simulation results include the tsunami-wave arrival time, the distribution of the maximum wave height, and the time series at free surface elevation.



▲ **Figure 3.** Band-pass filtered (period 20–50 s) three-component (left) observed and (right) synthetic displacement seismograms (top, middle, and bottom panels for vertical, transverse, and radial components, respectively). Each panel shows a profile of seismograms at epicentral distances between 32 and 550 km. Blue lines indicate the arrival time of *S* waves propagating at a speed of 4.2 km/s, whereas red and light blue lines indicate the arrival times of Rayleigh and Love waves propagating at 3.5 and 3.7 km/s, respectively.

**Frequency band: 0.02 - 0.05 Hz**

**Fitness: 1.035**



▲ **Figure 4.** Waveform fitting results. The gray scale represents different weighting coefficients based on signal-to-noise ratio (SNR) of individual observed waveforms. The station name, SNR value, time shift (shif), normalized waveform cross-correlation coefficient (CC), and variance reduction (VR) are given at the top of each trace. The epicentral distance (Epi.), station azimuth (Azi.), and maximum amplitude (Max. Amp.) are given at the bottom of each trace.

## SEISMIC OBSERVATION AND LANDSLIDE SOURCE INVERSION

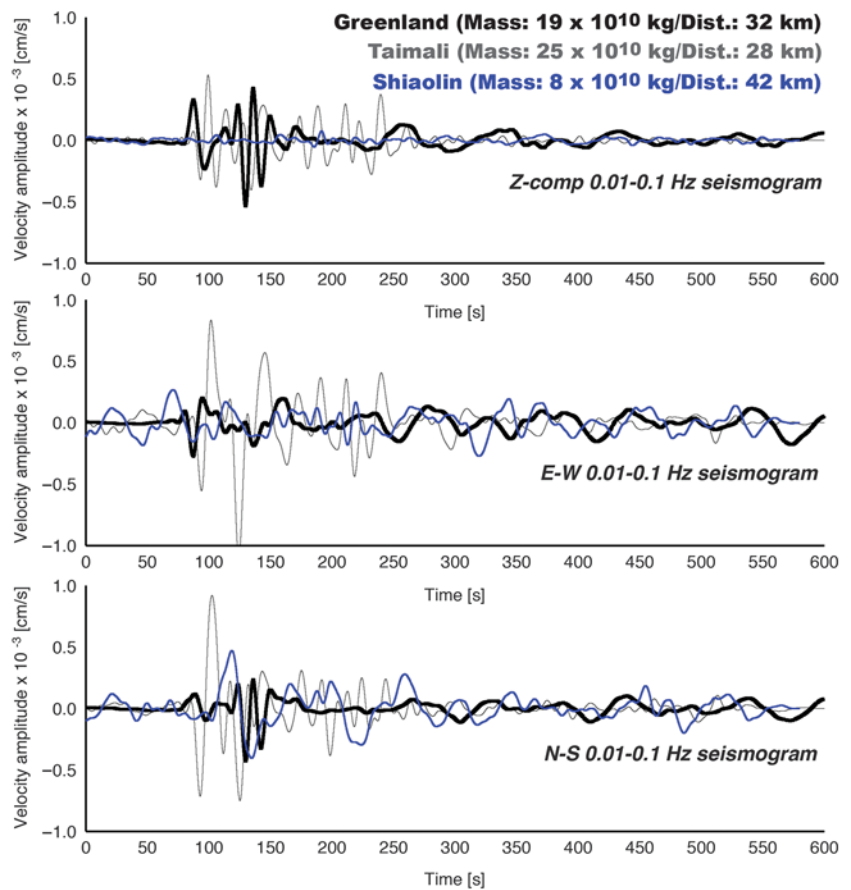
We obtained seismograms from the GLISN stations that recorded the ground motions following the Greenland landslide (records archived by the IRIS-DMC, see [Data and Resources](#)).

The profiles of LP waveforms recorded at stations located between 32 and 550 km from the landslide source definitely show signals from the landslide event (Fig. 3), with clearly identifiable *S* and surface waves. In general, LP seismic signals are generated by the sliding forces from the collapsed mass acting on the Earth's surface (Ekström and Stark, 2013). Before the

waveform inversion, we first compute the synthetic waveforms (Fig. 3) according to a single-force (SF) model, setting a sliding direction of 195° clockwise from north and a dipping angle  $\theta$  of 60°. In the forward modeling, we adopted a sinusoidal force–time function (unloading and reloading of landslide mass) with a duration of 30 s. Comparison of the synthetic and observed seismograms indicates that a point force alone cannot explain the source dynamics. Therefore, we also applied an inversion algorithm (Chao *et al.*, 2016) to derive the 3D LFHs using the three-component (radial, transverse, and vertical) LP records.

Previous studies (Chao *et al.*, 2016, 2017) have demonstrated that high-quality records from a few stations suffice to obtain a reliable solution (fitness > 0.75). For the Greenland event, our inversion yields a maximum absolute force ( $F_{\max}$ ) of  $2.903 \times 10^{11}$  N with a fitness value of 1.035 (Figs. 1c and 4). Application of a regression scaling relation linking the landslide seismic magnitude and  $F_{\max}$  value established by Chao *et al.* (2016) yields a landslide magnitude of 4.3, consistent with the preliminary 4.1 magnitude reported by the U.S. Geological Survey. The results of the 3D LFHs (Fig. 1c) show that the accelerating forces (upward vertical forces) due to mass unloading point toward the northeast. During the deposition stage (downward vertical forces), the decelerating forces due to mass reloading are directed to the southwest. These force directions are in agreement with the geometry of the landslide inferred from the Sentinel-2 images. We further estimated the collapse mass ( $m$ ) from the resulting LFH by assuming a time-independent  $m$ -value and ensuring that the block-mass trajectory (derived by twice integrating the 3D acceleration time series) fits the runout path mapped from the Sentinel-2 images (Figs. 1a and 2). Here, the acceleration time series are computed directly by dividing the LFHs by the collapsed mass. We found an  $m$ -value of  $1.9 \times 10^{11}$  kg, roughly consistent with the value of  $1.2 \times 10^{11}$  kg computed by the empirical equation  $m = 0.405 \times F_{\max}$  after Chao *et al.* (2016).

The seismic source inversion also provides crucial estimates of the physical parameters associated with the landslide event. Comparison between the timing of the relatively large velocity during the deposition stage and the position of the block mass along its trajectory (time progression shown in Fig. 1c with dots in different colors) suggests that the mass slumped into the sea immediately after sliding. The forces are primarily vertical, which is supported by the observation of a maximum velocity of 41.3 m/s in the vertical component (shown in Fig. 1d), and a high-dipping angle of the sliding force (shown with numerical labels in Fig. 1a). As a result,



▲ **Figure 5.** Comparison of waveforms from three different landslides, namely the Greenland (black), Taimali (gray), and ShiaoLin (blue) landslide events. Seismic analyses for the Taimali and ShiaoLin events have been presented previously (Chen *et al.*, 2013; Chao *et al.*, 2016).

the seismic amplitudes from the Greenland event are much larger in the vertical component than in the horizontal, in contrast to other landslides (Kanamori and Given, 1982; Brodsky *et al.*, 2003; Chao *et al.*, 2016) which exhibit stronger seismic radiations in the horizontal component (Fig. 5). In the case of subaerial landslide tsunamis, analytical studies have shown that a mass sliding down a hill with a dipping angle of 51.6° produces the highest tsunami waves (Heller and Hager, 2014). Consequently, the seismically determined source characteristics of the Greenland landslide, including its steep sliding angle and rapid moving velocity, seem very favorable to the generation of large tsunami waves, leading to high tsunami hazard.

## FORWARD TSUNAMI MODELING

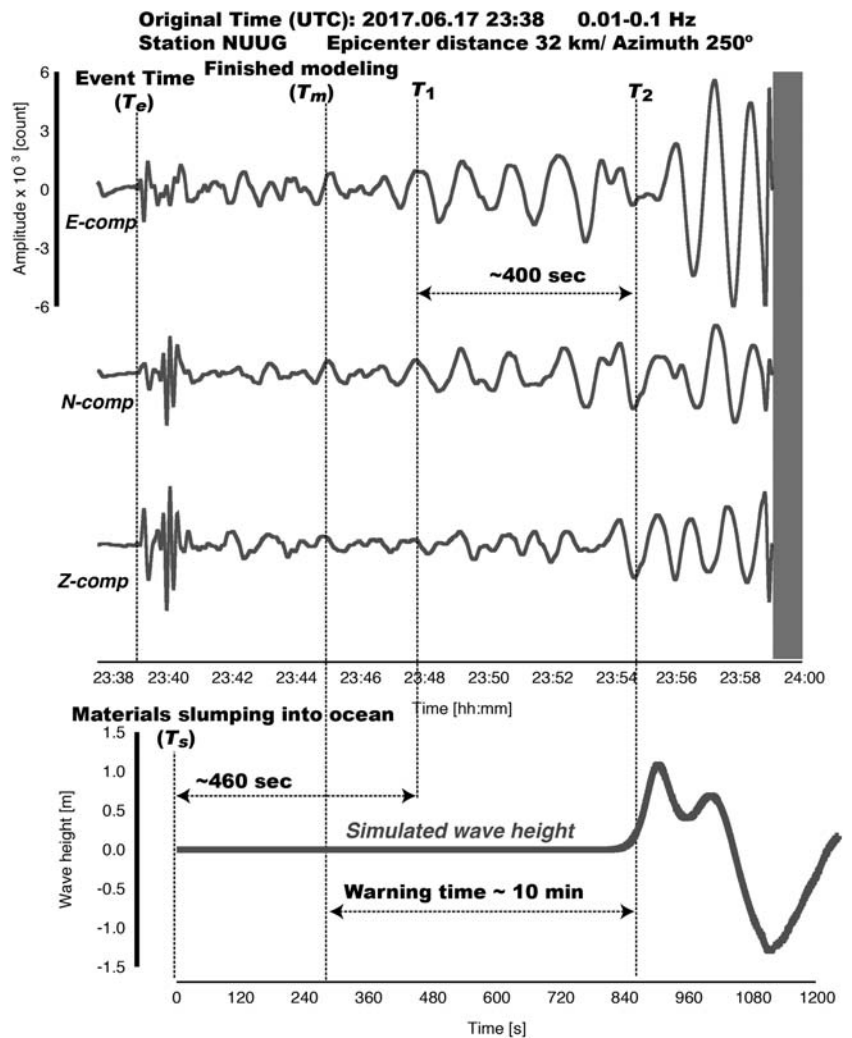
The volume of the sliding mass that enters the water is a key parameter for tsunami-wave simulation. With an estimated mass of  $1.9 \times 10^{11}$  kg, and assuming an average rock density of  $2500 \text{ kg/m}^3$ , we estimated landslide collapse volume of  $7.6 \times 10^7 \text{ m}^3$ . Based on the analysis of the differential DEM,

the volume of the accumulated material is  $1.6 \times 10^6 \text{ m}^3$  (Besette-Kirton *et al.*, 2017), indicating that a minimum material volume of  $7.44 \times 10^7 \text{ m}^3$  sliding into the seawater is conducive to tsunami generation. We conducted forward modeling of the tsunami-wave height at the village of Nuugaatsiaq with the initial wave height at the event location, and considered tsunami damage at the village of Nuugaatsiaq due to a tsunami-wave height of about 1 m as reference. The generation, propagation, and shoaling processes of the landslide-generated tsunami are simulated via the COMCOT model (Lin *et al.*, 2015).

Because direct observations of the tsunami near the village of Nuugaatsiaq, including tidal-gauge records, are lacking, the seismic records provide valuable information to validate the propagation of the tsunami wave. The broadband seismic station NUUG, located at the eastern end of the village, recorded clearly periodic seismic waves that grow both in amplitude and period (Fig. 6). This feature might be related to the ground motion induced by the tsunami waves. The larger amplitudes recorded on the east–west component are evident once we consider the westward propagation of the tsunami wavefront from the landslide source to the village, as shown in Figure 7a. Data from the NUUG seismic station were not usable after about 18 min of the landslide occurrence, probably due to a power failure and/or a telemetry loss caused by seawater washing up the village.

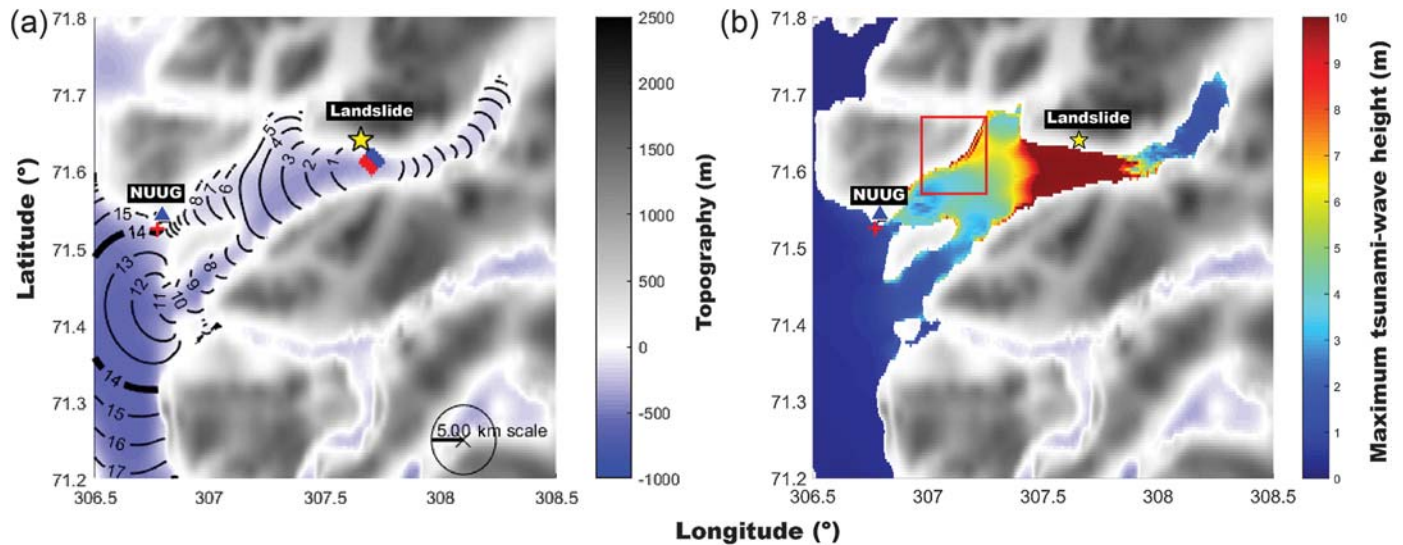
Considering a slump model for the initial wave height, the resulting maximum tsunami-wave height (MTWH) near the coast of the village can be estimated (Fig. 8a). For a volume of  $7.5 \times 10^7 \text{ m}^3$  and a slump length of 1500 m, equivalent to the trajectory shown in Figure 1a from landslide seismic modeling, we estimated a slump thickness of 33.5 m with an assumed slump width of 1500 m. Given the volume and geometry, an initial wave height of about 80 m leads to an MTWH of about 1.08 m near the coast of the village (Fig. 8a). Similarly, a field investigation also found that disturbances pushed the water levels about 90 m upward along the coastline of the landslide site (Schiermeier, 2017).

Using an initial wave height of 80 m in the offshore region near the landslide site in the tsunami simulation, we draw tsunami-wave travel-time isochrones from the event site to the village of Nuugaatsiaq, as shown in Figure 7a. As illustrated, the tsunami wave reaches the village  $\sim 14$  min after the slump. This time, identifiable in the simulated tsunami-wave time series (Fig. 8b), is close to the time when the periodic wave is observed at the seismic station NUUG ( $T_2$  label in Fig. 6).

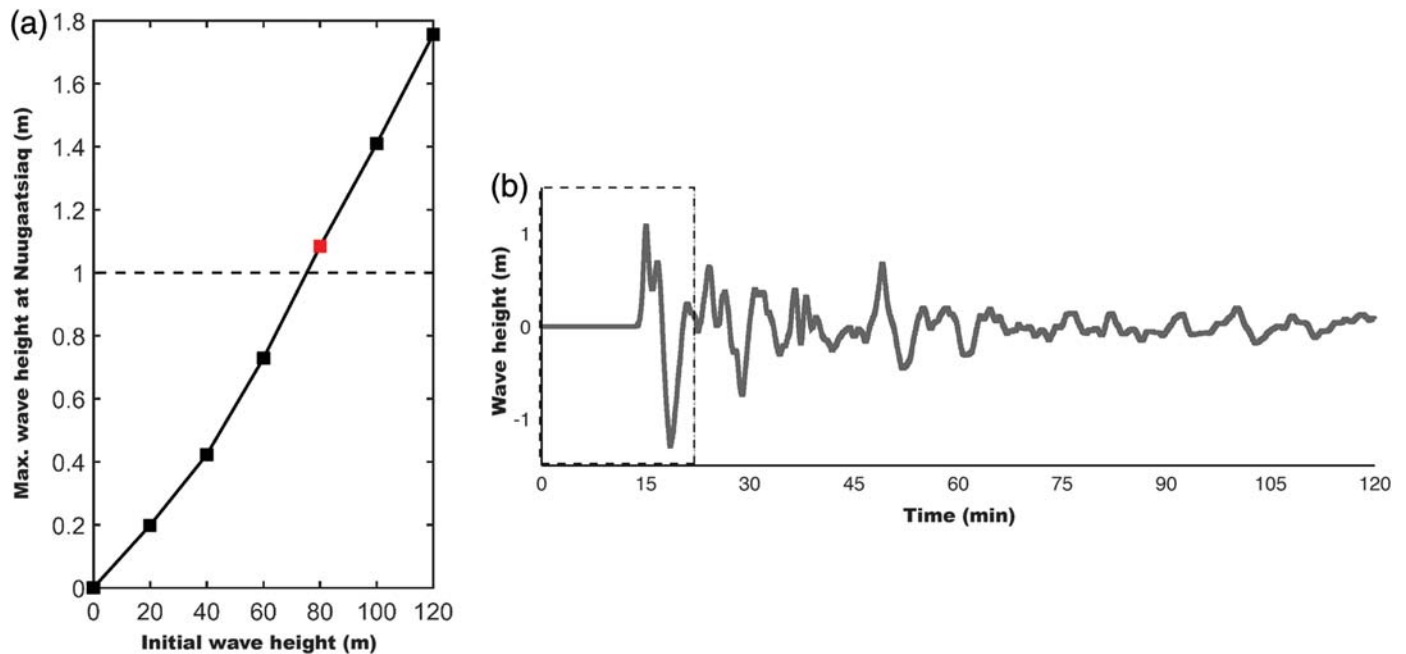


▲ **Figure 6.** Three-component seismograms recorded at (top) station NUUG and (bottom) simulated tsunami-wave height. Seismic records in the time interval covered by the thick gray-shaded area on the right are not usable. The time when the mass slumped into the sea ( $T_s$ ) and the event occurrence time ( $T_e$ ) were inferred from the LFH waveform inversion (Fig. 4) and recorded waveforms (Fig. 3), respectively. The 2-hr-long simulated tsunami-wave height is displayed in Figure 7.

Figure 6 also compares the simulated tsunami wave at the coast of the village with the three-component seismic records at the station NUUG. Figure 7b displays the MTWH in the tsunami-wave propagation area. The red rectangle in Figure 7b shows that the area has an MTWH of about 10 m, with an arrival time of 5–8 min. This implies that the area would suffer severe tsunami damage, but fortunately no tsunami damage was reported in that region. This large tsunami-wave height along the coast of the peninsula, however, could have contributed to the seismic waves recorded at the station NUUG, consistent with the observations ( $T_1$  label in Fig. 6). It also leads to differences in tsunami-wave travel times to the NUUG station.



▲ **Figure 7.** (a) Tsunami-wave travel-time isochrones predicted from the tsunami model with the initial wave of subsidence (blue) and uplift (red) near the landslide source (yellow star). The thicker contour shows the 14 min travel-time isochrone. (b) Simulated maximum tsunami-wave height (MTWH). The red rectangle shows hazardous wave heights in the northeastern part of the peninsula. Tones of red indicate the areas with larger tsunami-wave heights, whereas dark red illustrates wave heights larger than 10 m. The yellow star indicates the landslide source. The blue triangle shows the location of the NUUG seismic station. The red cross shows the location of the receiver location for which the tsunami-wave simulation result is shown.



▲ **Figure 8.** (a) MTWH as a function of initial wave height. Result used in the final explanation is shown by the red square. (b) Simulated tsunami-wave time series on the coast of the village of Nuugaatsiaq. The portion in the dashed rectangle is shown in more detail in Figure 6.

## CONCLUSIONS

The results obtained from the integration of seismic waveform inversion analysis and forward tsunami simulation in this study allow us to draw the following conclusions.

- Analysis of seismic data recorded by the GLISN network, located a few hundred kilometers from the Greenland landslide, could have rapidly detected the landslide. Moreover, the ground motions generated by the Greenland landslide and ensuing tsunami waves could have been

detected at the closest seismic station NUUG. This could have led to an actionable real-time tsunami warning without direct measurements of water waves (Fig. 6).

- Seismic waveform inversion provides an estimate of the landslide volume of  $7.6 \times 10^7 \text{ m}^3$ , which is larger than the geodetic estimate of  $5.0 \times 10^7 \text{ m}^3$  (Bessette-Kirton *et al.*, 2017) by a factor of about 1.5. This discrepancy could result from the limited applicability of our seismic model, based on the assumption of a simple block mass, and/or the limited spatial resolution of the satellite images.
- Under the assumption that most of the landslide material slid into the ocean, our simulated tsunami waves reach a height of up to 80 m, roughly consistent with the field observations (Schiermeier, 2017). Considering the propagation time of the hazardous tsunami waves (14 min inferred from tsunami simulation) and seismologically inferred timing of the landslide mass slumping into the seawater, a lead time of 10 min could have been achieved for the town of Nuugaatsiaq (Fig. 6).
- Although seismic data analysis alone cannot yield the volume of the sliding materials involved in the slumping, it does provide a constraint on the upper limit of the volume of the slumping material. This can lead to false alarms because the simulation of the tsunami waves takes into account the total landslide mass. In such cases, we can use sea level measurements provided by stations located in the vicinity of the landslide site as a reference to refine the tsunami-wave prediction in the targeted coastal area.
- For the Greenland landslide, in hindsight, we determined the source characteristics via seismic analysis 6 min after origin time. With knowledge of the landslide location and volume, we could then model the potential tsunami-wave height induced by landslides near coastal regions and issue warnings shortly after the events.
- In the practice of real-time monitoring, once the seismic waves from the landslide reach a minimum number of stations, source location and event origin time could be estimated applying a grid-based SF inversion (Chao *et al.*, 2017). To determine the location more accurately, we can further relocate the source location by maximizing the coherence of the seismic horizontal envelope functions at the stations, with a source location error of 2 km or less (Chen *et al.*, 2013). The landslide volume could then be estimated directly via waveform inversion. The entire process of location and volume determination takes only a few seconds. The lead time for a tsunami warning will depend mainly on the length of seismic records used in the inversion.
- In Taiwan, the above-mentioned processes have been implemented in a near-real-time landslide monitoring system (NRLMS, Chao *et al.*, 2017; see Data and Resources) relying on a real-time broadband seismic network. The NRLMS operates as a fully automatic detection system that delivers quick reports containing the source param-

eters (e.g., event time, location, force mechanism, and volume) to users via e-mail. The system can also identify the landslide source by examining the fitness parameters of the waveform inversion for different types of source mechanisms and can easily be adopted in other places in the world with a high landslide hazard potential using the real-time GSN.

## DATA AND RESOURCES

Seismic waveforms of the Greenland Ice Sheet Monitoring Network (GLISN, <http://www.iris.edu/hq/programs/glisn>, last accessed February 2018) used in this study were obtained from the Incorporated Research Institutions for Seismology Data Management Center (IRIS-DMC, <http://ds.iris.edu/ds/nodes/dmc/data/>, last accessed July 2017). The Sentinel-2 satellite images are open to the public and can be obtained upon request from the European Space Agency (ESA) Earth Online (<https://earth.esa.int/web/guest/missions/esa-operational-eo-missions/sentinel-2>, last accessed July 2017). The video taken by a villager used in this study is at <https://www.youtube.com/watch?v=LzSUDBbSsPI> (last accessed July 2017). The bathymetric data can be accessed directly at <http://www.gebco.net/> (last accessed July 2017). The near-real-time landslide monitoring system (NRLMS) has been online operated at <http://collab.cv.nctu.edu.tw/main.html>. The software package Generic Mapping Tools (GMT, Wessel and Smith, 1998) was used to make some of the figures in this article. ☒

## ACKNOWLEDGMENT

This research has been supported by the Ministry of Science and Technology (MOST) of Taiwan.

## REFERENCES

- Allstadt, K. (2013). Extracting source characteristics and dynamics of the August 2010 Mount Meager landslide from broadband seismograms, *J. Geophys. Res.* **118**, 1472–1490, doi: [10.1002/jgrf.20110](https://doi.org/10.1002/jgrf.20110).
- Bessette-Kirton, E., K. Allstadt, J. Pursley, and J. Godt (2017). Preliminary analysis of satellite imagery and seismic observations of the Nuugaatsiaq Landslide and Tsunami, Greenland, *U.S. Geological Survey—Landslide Hazards Program*, available at <https://landslides.usgs.gov/research/featured/2017-nuugaatsiaq/> (last accessed November 2017).
- Brodsky, E. E., E. Gordeev, and H. Kanamori (2003). Landslide basal friction as measured by seismic waves, *Geophys. Res. Lett.* **30**, no. 24, 2236, doi: [10.1029/2003GL018485](https://doi.org/10.1029/2003GL018485).
- Chao, W. A., Y. M. Wu, L. Zhao, H. Chen, Y. G. Chen, J. M. Chang, and C. M. Lin (2017). A first near real-time seismology-based landslide monitoring system, *Sci. Rep.* **7**, 43510, doi: [10.1038/srep43510](https://doi.org/10.1038/srep43510).
- Chao, W. A., L. Zhao, S. C. Chen, Y. M. Wu, C. H. Chen, and H. H. Huang (2016). Seismology-based early identification of dam-formation landslide events, *Sci. Rep.* **5**, 19259, doi: [10.1038/srep19259](https://doi.org/10.1038/srep19259).
- Chen, C. H., W. A. Chao, Y. M. Wu, L. Zhao, Y. G. Chen, W. Y. Ho, T. L. Lin, K. H. Kuo, and R. M. Zhang (2013). A seismological study of earthquakes using a real-time broad-band seismic network, *Geophys. J. Int.* **194**, 885–898.
- Costa, J. E., and R. L. Schuster (1988). The formation and failure of natural dams, *Geol. Soc. Am. Bull.* **100**, 1054–1068.

- Drusch, M., U. Del Bello, S. Carlier, O. Colin, V. Fernandez, F. Gascon, B. Hoersch, C. Isola, P. Laberinti, P. Marimort, *et al.* (2012). Sentinel-2: ESA's optical high-resolution mission for GMES operational services, *Remote Sens. Environ.* **120**, 25–36.
- Ekström, G., and C. P. Stark (2013). Simple scaling of catastrophic landslide dynamics, *Science* **339**, no. 6126, 1416–1419, doi: [10.1126/science.1232887](https://doi.org/10.1126/science.1232887).
- Heller, V., and W. H. Hager (2014). A universal parameter to predict subaerial landslide tsunamis? *J. Mar. Sci. Eng.* **2**, 400–412.
- Kanamori, H., and J. W. Given (1982). Analysis of long-period seismic waves excited by the May 18, 1980, eruption of Mount St. Helens—A terrestrial monopole? *J. Geophys. Res.* **87**, 5422–5432.
- Kennett, B. L. N., E. R. Engdahl, and R. Buland (1995). Constraints on seismic velocities in the Earth from traveltimes, *Geophys. J. Int.* **122**, no. 1, 108–124.
- Lin, S. C., T. R. Wu, E. Yen, H. Y. Chen, J. Hsu, Y. L. Tsia, and L. F. L. Philip (2015). Development of a tsunami early warning system for the South China Sea, *Ocean Eng.* **100**, 1–18.
- Poli, P. (2017). Creep and slip: Seismic precursors to the Nuugaatsiaq landslide (Greenland), *Geophys. Res. Lett.* **44**, 8832–8836, doi: [10.1002/2017GL075039](https://doi.org/10.1002/2017GL075039).
- Schiermeier, Q. (2017). Huge landslide triggered rare Greenland megatsunami, *Nature* doi: [10.1038/nature.2017.22374](https://doi.org/10.1038/nature.2017.22374).
- Wessel, P., and W. H. F. Smith (1998). New, improved version of Generic Mapping Tools released, *Eos Trans. AGU* **79**, 579.
- Zhu, L., and L. A. Rivera (2002). A note on the dynamic and static displacements from a point source in multilayered media, *Geophys. J. Int.* **148**, 619–627.

*Wei-An Chao*  
*Department of Civil Engineering*  
*National Chiao Tung University*  
*No. 1001, Daxue Road, East District*  
*Hsinchu 30010, Taiwan*  
*vnchao@nctu.edu.tw*

*Tso-Ren Wu*  
*Meng-Ju Chung*  
*Yu-Lin Tsai*

*Institute of Hydrological and Oceanic Sciences*  
*National Central University*  
*No. 300, Zhongda Road*  
*Jhongli 32001, Taiwan*

*Kuo-Fong Ma*  
*Department of Earth Sciences*  
*National Central University*  
*No. 300, Zhongda Road*  
*Jhongli 32001, Taiwan*

*Yu-Ting Kuo*  
*Li Zhao*  
*Institute of Earth Sciences*  
*Academia Sinica*  
*No. 128, Section 2, Nankang District*  
*Taipei, 11529, Taiwan*

*Yih-Min Wu*  
*Department of Geosciences*  
*National Taiwan University*  
*No. 1, Section 4, Roosevelt Road, Da'an District*  
*Taipei 10617, Taiwan*

*Han Wu<sup>1</sup>*  
*Seismological Observation Center*  
*Central Weather Bureau*  
*No. 64, Gongyuan Road*  
*Taipei 10048, Taiwan*

Published Online 25 April 2018

<sup>1</sup> Also at Institute of Hydrological and Oceanic Sciences, National Central University, No. 300, Zhongda Road, Jhongli 32001, Taiwan.